THE INFLUENCE OF MORPHOLOGY AND CRYSTAL ORIENTATION OF SPANGLES ON HOT-DIP Zn-0.5Sn ALLOY COATING

L. Zhai [a], H.-P. Peng [a,b,c,*], Y. Liu [b,c], Y. Lei [a], S. Deng [a], X.-P. Su [b,c]

[a] Jiangsu Key Laboratory of Oil & Gas Storage and Transportation Technology,
Changzhou University, Jiangsu, P.R. China
[b] Jiangsu Key Laboratory of Material Surface Science and Technology,
Changzhou University, Jiangsu, P.R. China
[c] Jiangsu Collaborative Innovation Center of Photovoltaic Science and Engineering,
Changzhou University, Jiangsu, P.R. China

Abstract

The study on the surface morphology and crystal orientation of the Zn-0.5Sn coating could offer some guidance to improve the surface performance of the hot-dip galvanizing coating. In this paper, a scanning electron microscope (SEM) and an energy dispersive spectrometer (EDS) were used to analyze the typical morphology and the element distribution of spangles. The surface texture of the coating was analyzed by X-ray diffraction (XRD). Electron backscatter diffraction (EBSD) was used to analyze the crystal orientation of spangles. The results show that Sn segregates among the spangle dendrites while a metastable divorced eutectic structure can be maintained in the tin-rich phase, where the composition tends to be very similar. The crystal orientation of spangles affects their morphology, leading to the formation of feathery, ridged, and orthogonal dendrite arm spangles. When the angle among the <0001> orientation of the spangle crystal and the normal of the steel base surface changes from 0° to 90°, feathery spangles change to orthogonal dendrite arms spangles. The misorientation within a spangle is small while that among spangles is quite large. The orientation changes in the direction of the dendrite arm are relatively smooth and low, while the orientation changes which are perpendicular to the dendrite arm have a saltatory and irregular fluctuation.

Keywords: Hot-dip galvanizing; Spangle; Crystal orientation; Backscattered electron diffraction

1. Introduction

Hot-dip galvanizing is a common method of providing corrosion resistance for steel materials. The striped steel was immersed in molten zinc to obtain a protective zinc layer [1, 2]. With certain alloy elements (such as Sn, Sb, Pb, Bi) added to the molten zinc [3, 4], a pattern of uneven, light, and dark interlacing and dense dendrites will form on the surface of the zinc layer. The dendrites are called spangles, a kind of crystal grains that are large enough to be seen by naked eyes. A single spangle is usually composed of one or multiple feathery, bright, pit-like, ridge-like, or orthogonal dendrite arm morphologies [5]. Spangles can be considered as a symbol of high-quality coating. However, requirements for surface smoothness have been continuously improved with the advance of the automotive and home appliance industries. The uneven spangles morphology hinders industrial production. Therefore, it is necessary to systematically study the surface spangles morphology.

Studies on spangles have been carried out a long time. J. Strutzenberger et al. [5] found that the Zn-Pb coating has bright, dark, feathery, and ridged spangle through an optical microscope (OM) and SEM. They drew a schematic diagram of the crystal orientation of spangles. Their morphology is thus found to be associated with orientation. According to A. Sémoroz et al., through EBSD measurement and kinetic analysis of the dendrite growth of the Zn-Pb spangle, the growth rate of the zinc dendrite is related to the spangles morphology and the solid-liquid interface energy during solidification [6]. Later research proved that the orientation domain [7] exists and that the zinc coating has a significant (0001) texture. M. Zapponi et al. [8] found that the addition of a small amount of Sb in the molten zinc would cause serious surface segregation. Few Sb was found on the surface of feathery spangles, while high Sb content was found

on the dark spangles surface. The segregation of Sb influences the morphology as well as the size of spangles. A. Sémoroz et al. [9] used EBSD and OM to study the morphology and orientation of the 55Al-43.4Zn-1.6Si coating. The surface coating is different from that of bright and dark spangles of the Zn-Pb, which only has dendritic α-Al morphology. Besides, the crystal orientation within a single grain leads to a significant change. Wang Xinhua et al. discovered the morphology of the Zn-0.2Sb spangle and its orientation by the x-ray diffraction (XRD) crystal transformation method [10]. As a result, they found the formula relationship among the angle of the spangle dendrite arm [11]. Rex Y. Chen and Daniel Yuen [12] studied morphology and crystal orientation of the 55Al-43.4Zn-1.6Si coating using EBSD, XRD, OFD density distribution function, pole table, etc. The study shows that the coating surface has a center-symmetrical dendrite morphology. Meanwhile, (111) and (100) are the most common orientations in the coating. Peng Shu et al. [13-16] analyzed different morphologies of spangles and the surface roughness of Zn-Pb coating by atomic force microscopy. According to their research, the dark spangle with the most segregation of Pb on the surface has the highest roughness.

Many studies have been conducted on the Zn-Pb and Zn-Sb spangle, but there are rare studies on the Zn-Sn spangle coating. Compared with Pb, Sb, and Bi, Sn produces smaller spangle [17, 18] (When the amount is 0.2 wt.%, the size is only about 1.2 mm). Researches on the morphology and crystal orientation can contribute to studying smooth and easy-to-print spangle materials. This study focuses on the use of EBSD to analyze the different crystal orientations in the Zn-0.5Sn alloy coating and the influence of segregation of Sn on the coating surface towards the spangles morphology. The reasons for the influence will be discussed in this paper.

2. Experimental methods

After degreasing the carbon steel sheets in 15 wt.% NaOH, pickling with 10 wt.% HCl, we put them in 15 wt.% $ZnCl_2$ + 15 wt.% NH_4Cl solution and dried the 20# high-quality carbon steel sheet specimen (weight percentage of component: C, 0.19; Si, 0.29; Mn, 0.42; P, 0.031; S, 0.029; Cr, 0.19; Ni, 0.22; Cu, 0.18) with a size of 60×40×1.2 mm. It was galvanized in a bath of Zn-0.5Sn in a hot-dip galvanizing simulator at 450°C. The steel plate was kept in the zinc bath for one minute. The hot-dip galvanizing simulator was modified from an intermediate frequency furnace to maintain a stable temperature. When entering or withdrawing the zinc bath, an additional robot scraped the zinc dust off the surface to keep the sample surface clean. Meanwhile, an air

knife system was adopted to prevent overcoating. Clear spangle regions were cut down after being detected by OM. SEM and EDS were employed to study the typical surface morphologies and the distribution of Sn on the surface of spangles. The composition reported herein is the average of at least five measurements of five congeners. The texture of the coating was studied by XRD patterns generated by a D/max 2500 PC X-ray diffractometer with Cu Ka radiation and a 2θ angle step of 0.02°. Si powders were used as external calibrated standards. Jade software package was used to index and calculate the XRD patterns.

EBSD analyzed the influences of spangle orientation and Sn segregation of the surface morphology. The sample was lightly polished to keep a trace of the surface roughness and adhered to the sample holder with the conductive tape. The tilt of the sample holder was adjusted to 70°. The Euler angles φ_1, Φ, and φ_2 were all set as 0 in the CS0-CS1 transition to formulate the sample coordinate system. Besides, the accelerating voltage of the SEM was 20 kV, and the scanning step was 20 μm. After removing the noise through Tango software, the orientation distribution map was obtained, where the crystal orientation of each point was represented by different false colors. In addition, the misorientation of crystal grains and dendrites were measured by the misorientation tool. The preferred orientation distribution of the sample was obtained by drawing pole figures of three viewing angles in Mambo software. For the sake of data accuracy, all samples were tested three times.

3. Results and discussion
3.1 Microstructure of spangles of Zn-0.5Sn alloy coating

After adding 0.5 wt.% Sn to the molten zinc, many spangles would appear on the surface of the hot-dip galvanized steel sheet. Figures 1-4 show the backscattered electron images of four typical morphologies of spangles.

Figure 1 (a) shows the backscattered electron image (BSE) of feathery spangles. According to the figure, there are six symmetrically distributed primary feathery dendrite arms. The lath-shaped secondary dendrite arms and the primary dendrite arms present a 60° angle, distributed in parallel. Many scholars view the shiny spangle as a separate branch, but it is a relatively flat and bright area in the feathery spangle, as shown in the upper part of Figure 1 (b). The grooves among the dendrites are as shown in Figure 1 (c). No obvious tin-rich phase was observed on the surface of the feathery spangle, but some acicular tin-rich phases were found among the dendrites in the enlarged image in Figure 1 (c). As indicated by the

arrows in the high magnification BSE Figure 1 (d), it is obvious that the acicular phases (1) protrude from the base surface. The average composition of tin-rich phases is shown in Table 1. The numbers in the figure refer to different phases in order, corresponding to the components in Table 1.

The BSE of the feather-grain divided spangle is shown in Figure 2 (a), where the spangle is relatively bright and flat on the lower right side, with almost no Sn segregation. On the upper left side, there is a dim and rough granular structure with a large amount of Sn segregation. Like feathery spangles, acicular tin-rich phases exist among dendrites in feathery regions (2), as indicated by the arrows in Figure 2 (b). The image of the backscatter also proves the convex spangles morphology. There are a lot of dense dark gray granular structures in the upper left corner, composed of pure Zn. In the enlarged BSE of the dark gray granule structure, there are many white acicular (3) and bulk phases (4) in the granule grooves (Figure 2 (c)). Meanwhile, the average composition of these phases is shown in Table 1. EDS data show that much lower tin content is discovered in the acicular phase than the bulk phase. In addition, the BSE (Figure 2 (c)) shows no convex morphology in the bulk phase. The BSE of the high-magnification bulk (Figure 2 (d)) has a single white phase instead of a typical layered eutectic structure.

Figure 3 (a&b) shows the BSE of the ridged spangle in the transitional state among the feathery spangle and the orthogonal dendrite arms spangle. From this figure, spangles in the upper and lower areas have a lath-like structure, which is similar to that of feathery spangles. On the contrary, spangles in the left and right areas have the fish-scale structure like their structure in granular areas. There are many white bulk tin-rich phases (5) in the lath-structured area,
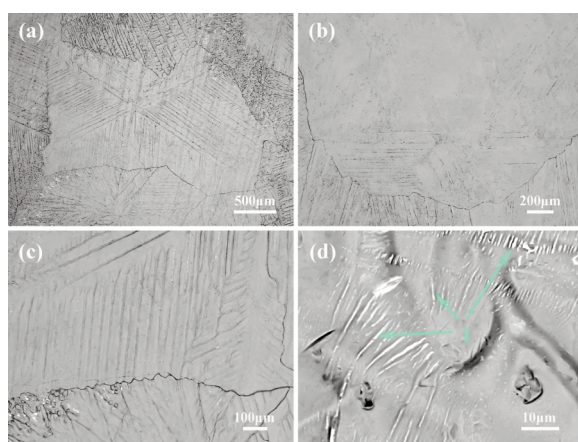
linearly distributed in the dendrite arm grooves (Figure 3 (c)). In the fish-scale structure area, there are a few white bulk Sn-rich phases distributed in the dendrite arm grooves (6) and among the dendrite arms (7) (Figure 3 (d)). The average composition of the tin-rich phase is shown in Table 1.

Figure 4 (a&b) shows the BSE of the orthogonal dendrite arm spangle. For these spangles, two vertically intersecting primary dendrite arms are formed first, and then the secondary dendrite arms, which are orthogonal to the primary ones, continue to grow in that direction. Due to nucleation dynamics [5], there is a difference between the horizontal and vertical dendrite growth rates. Thus, the secondary dendrite growth is inhibited in the inferior direction. There are many white Sn-rich bulk phases (8) among dendrites on the left (Figure 4 (c)), while the tin-rich
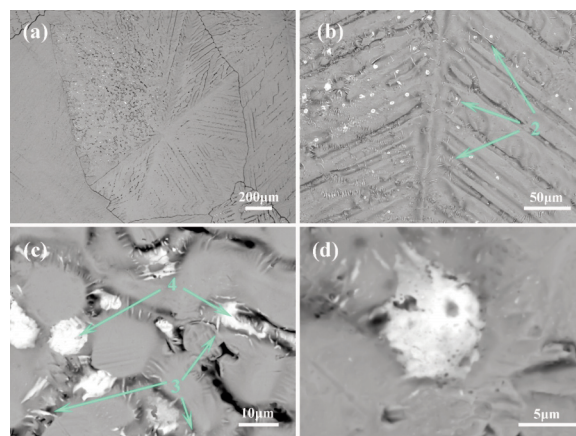

Figure 2. *Microscopic morphologies of the feather-grain divided spangles: (a) BSE of a feather-grain divided spangle; (b) BSE of the acicular phases among the dendrites; (c) BSE of the bulk phases in the granule grooves; (d) high magnification BSE of a bulk phase*
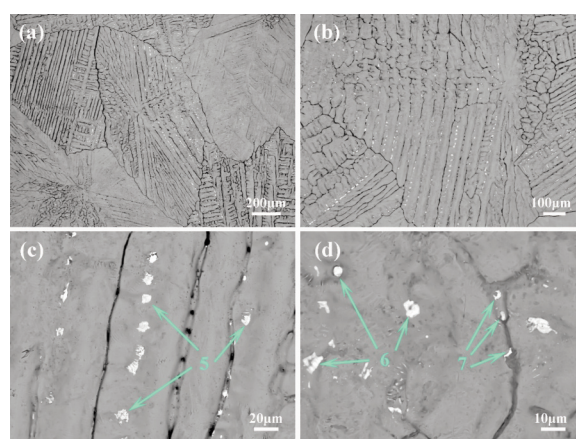

Figure 1. *Microscopic morphologies of feathery spangles: (a) BSE of a feathery spangle; (b) BSE of a "shiny" spangle; (c) BSE of the grooves among dendrites; (d) high magnification BSE of the acicular phases*

Figure 3. *Microscopic morphologies of ridged spangles: (a&b) BSE of ridged spangles; (c) BSE of the bulk phases in the lath-like area; (d) BSE of the bulk phases in the fish-scale area*

phases are striped on the right (9) (Figure 4 (d)). The composition of tin-rich phases is shown in Table 1. Since the compositions of the strip phase and the bulk phase are similar, it is believed that as the surface tin content increases, the tin-rich phase will change from bulks to strips. A detailed analysis of the eutectic structure will be discussed in the following part.

According to the four morphologies of spangles in Figures 1-4, the segregation of Sn on the coating surface is the main factor causing the different morphologies. In bright spangle regions and feathery spangle regions, there was almost no Sn on the surface. With the increase of Sn content, feather-grain divided spangles, ridged spangles, and the orthogonal dendrite arm spangles with the highest Sn content come into being in turn. Based on the data analysis of EDS, it is found that the tin content is low in the acicular tin-rich phase of the feathery area (12.4-22.8 wt.%), while that in the bulk and strip-shaped tin-rich phases tends to be similar, both less than the composition of eutectic point of 91.2 wt.% (85.1 at.%). According to the binary phase diagram of Sn-Zn (Figure 5), the tin-rich phase should have a eutectic structure. However, as shown in the backscattered picture, the tin-rich phase is white without having an obvious lamellar eutectic structure. Meanwhile, the tin content is significantly lower than 91.2 wt.%. That is because the designed composition of the zinc bath is Zn-0.5Sn, which is hypoeutectic. According to the phase diagram, the initial crystalline phase of Zn precipitates first during cooling. When the liquid phase components reach the eutectic point, the eutectic structure will be thereby formed. Based on the phase equilibrium data [19], the maximum solid solubility of Sn in Zn is 0.039 at.% while that of Zn in βSn is 0.6 at.% at the eutectic temperature(198.5°C). Therefore, it can be

approximated that the two phases are not mutually soluble. According to the lever theorem, the mass percentage of the primary Zn phase is 99.4%, while that of the eutectic structure is 0.6%. In a few cases of eutectic structures, the Zn phase is attached to the dendrite growth of the primary crystalline phase of Zn, so that the characteristics of the eutectic structure disappear and appear in the form of divorced eutectic. The coating is cooled under air conditions, which could be unbalanced. Due to the overcooling, the tin content of the eutectic structure is low (<91.2 wt.%),

Table 1. *Compositions of the tin-rich phases*

| Spangles morphology	Morphology of tin-rich phase	Composition(wt.%)	
		Zn	Sn
feathery spangle	acicular among dendrites (1)	77.2	22.8
feather-grain divided spangle	acicular among dendrites (2)	87.6	12.4
ridged spangle	acicular among granules (3)	46.4	53.6
	the bulk among granules (4)	38.1	61.9
	the bulk on dendrites (5)	69.7	30.3
	the bulk on fish scales (6)	43.5	56.5
orthogonal dendrite arm spangle	the bulk among fish scales (7)	46.3	53.7
	the bulk among dendrites (8)	43.0	57.0
	strip among dendrites (9)	47.9	52.1

The number is correlated with the figure 1-4.
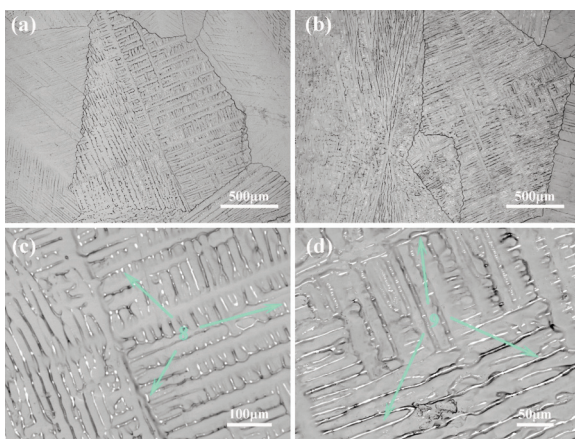
Figure 4. *Microscopic morphologies of the orthogonal dendrite arm spangles: (a&b) BSE of orthogonal dendrite arm spangles; (c) BSE of bulk phases among the dendrites; (d) BSE of strip phases among the dendrites*
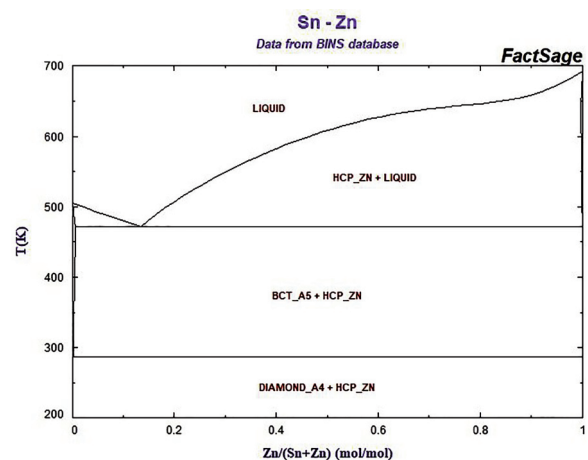

Figure 5. *Sn-Zn phase diagram, Source: Thermochemical data of FactSage*

so the structure would be denatured and metastable.

The tin-rich phase is the final solidified structure, so it is generally distributed in the dendrite arm grooves and among the dendrite arms. When there is little tin-rich residual liquid, because of the surface tension, it will exhibit different morphologies of the solid primary Zn phase. The acicular shape is caused by a slope in the granular primary Zn. Meanwhile, the tin-rich liquid is discharged during the solidification process of the granular crystalline phase of primary Zn. Next, the tin-rich liquid flows down the granular dendrite [20-22]. Due to the poor wettability between the tin-rich liquid and the primary Zn phase, the contact angle of the liquid-solid interface is large. Therefore, a raised and contracted acicular phase is produced during the solidification process of residual liquid. In the relatively flat upper surface of the dendrites, due to the surface tension, the tin-rich solution shrinks and presents a spherical crown.

In contrast, in the narrower dendrites, the tin-rich liquid fills the grooves, as shown in Figure 4 (c&d). Since both are orthorhombic dendrite arm spangles in Figure 4 (c&d), there is no substantial difference between them. From the data in Table 1, the surface segregation makes the surface Sn content much higher than that in the zinc bath. The amount of the surface tin-rich phase depends on the amount of eutectic residue at the end of solidification. Before solidification, the surface Sn content in the corresponding spangle region is in proportion to the eutectic residue to be obtained. Thus, the sub-grain boundaries can be better filled, and the originally isolated tin-rich phases can be connected into lines.

It is believed that the addition of Sn in the zinc bath will cause intergranular corrosion [23, 24]. However, on the spangle surface, the tin-rich phases are rarely distributed at the grain boundary, but more often to be seen at the sub-grain boundary (among dendrite arms), at least in the free zinc layer.

3.2 The effect of grain orientation on spangles morphology

The surface of hot-dip pure zinc is bright and smooth, with a dense concentration of small grains on it, as shown in the optical microscope Figure 6. Unlike the dendritic spangles morphology, these grains are smoother with some defects [25-27]. After tin is added into the zinc bath, the bright surface will be replaced by the spangle's morphology. When it comes to the cause of the huge changes on the coating surface, it was found to be related to the addition of Sn, which greatly changed the crystal orientation of η-Zn. The preferred orientation caused a huge variance in morphology. Figure 7 (a) 1shows the XRD diffraction pattern of high-purity zinc powder, which is in accordance with the standard pattern of zinc. The

pattern reflects that zinc has the most (10-11) crystal planes in the disordered condition, followed by (0002) planes and that the (10-10) planes were the third most ones. Two $10*10$ mm^2 parts were randomly selected and cut from the pure zinc coating, where relatively clear grains can be observed, for XRD analysis. The XRD patterns are shown in Figure 7 (a) 2, 3. Based on these patterns, it can be observed that the orientation of the pure zinc coating is much consistent with that of the zinc powder, while the peak intensity ratio is consistent with that of a standard pattern. In other words, the pure zinc coating does not have a preferential orientation, and the dense small grains are randomly oriented.

Four samples with relatively clear spangles morphology were chosen in a random manner. An area of $10*10$ mm^2 each was cut for XRD analysis. The pattern is shown in Figure 7 (b). Comparing the diffraction patterns of the four samples in the figure with those of standard zinc, we can find that the general matches of the diffraction angle positions, but the peak intensity ratio does not correspond to each other. Some weak peaks even disappeared in the samples. As shown in pattern 1, the strongest diffraction crystal plane (10-11) in the standard pattern becomes the stronger peak; the stronger diffraction crystal plane (0002) in the standard pattern becomes the strongest; and the remaining diffraction peaks almost disappear. It is a similar case in pattern 2-4. The (0002) plane becomes the strongest peak, while the weaker (10-10) becomes the stronger peak. The other diffraction peaks almost disappear. The diffraction peak of the (10-13) crystal plane in pattern 1-3 disappeared. Thus, the surface of the coating has a preferred orientation of <0002> and <10-10>. Therefore, it can be proved that the addition of Sn leads to a preferred orientation of the coating surface.

For further analysis on the corresponding relationship among orientation and spangles morphology, an area with several typical spangles
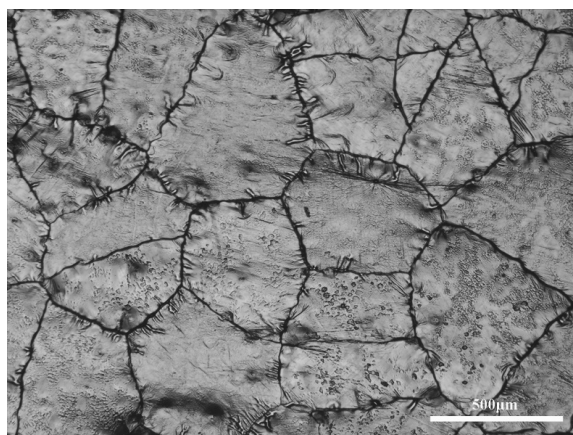

Figure 6. *Optical microscope photo of the pure zinc coating surface*

morphology was selected by EBSD. Due to the uneven surface of the spangles and high requirements of EBSD on the surface of the sample, there are many noisy points in this area. After removing the singular points and noisy points, the grain orientation distribution of spangles in Euler space is as shown in Figure 8 (a), where different false-color regions correspond to different grain orientations (marked with white numbers 1-8), and black curves refer to boundaries of the spangles. The small grains in the spangles are misjudged. Besides, white areas are zero-resolution areas due to the uneven surface. The corresponding micro-morphology of this area is shown in Figure 8 (b), where typical orthogonal dendritic arm spangles are in regions 1, 5, 7, and 8, ridged spangles in region 2, and feathery spangles in regions 3, 4, and 6. The false colors of the eight areas are all different, indicating that the grain orientations are also different among the spangles in these eight areas.

In order to analyze the preferred orientation of different types of spangles in the spatial direction, the direct pole figure method was used. The positive pole figures <0001>, <11-20>, and <10-10> crystal direction were obtained through the hemispherical projection method [28]. The rolling direction of the steel is defined as X_0, and the lateral direction is defined as Y_0. The projection shows on the lower hemisphere, as shown in Figure 9.

According to the pole figure of (0001) crystal plane, the feathery spangle (region 3) marked by fluorescent green is located at the center of the pole figure, which indicates that the orientation of the spangle <0001> is perpendicular to the plane of the steel. In region 3, there is an almost perfect feathery spangle whose angle of the primary dendrite arm is 60°. Meanwhile, the color spots of regions 4 and 6, which represent the feathery spangle as well, deviate slightly from the center. The result indicates that the <0001> orientation of these two spangles deviates
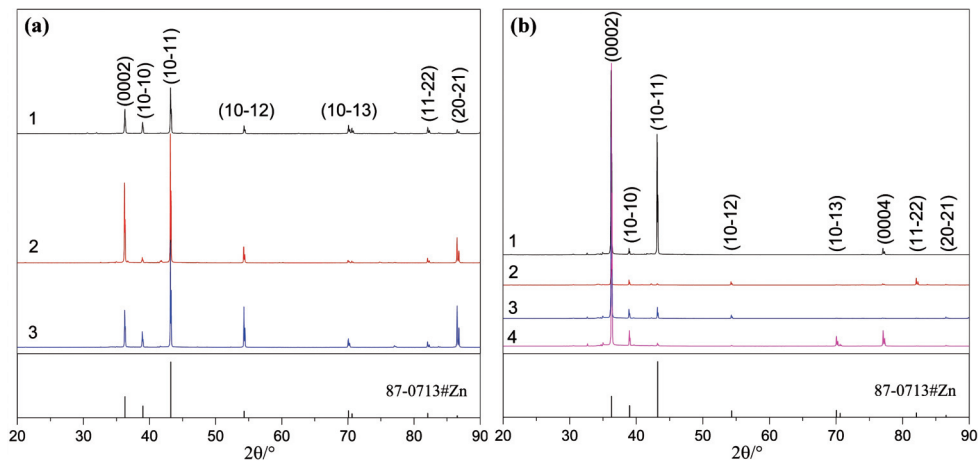

Figure 7. *X-ray diffraction patterns of (a) high-purity zinc powder and two plate samples of pure zinc coating; (b) four plate samples of Zn-0.5Sn coating*
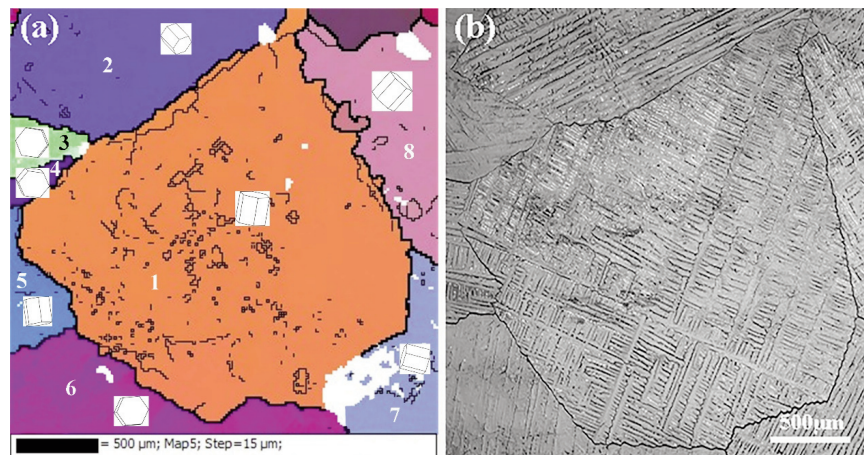

Figure 8. *(a) Orientation distribution map of spangles in different regions; (b) Backscattered electron image of selected spangle areas*

slightly from the normal direction of the steel base surface. According to the pole figure of (10-10) crystal planes, the false colors fluorescent green, dark blue, and deep purple spots representing the regions 3, 4, and 6 (feathery spangle) form into three spots with 60° angles distributed on the circumference. This is consistent with the hexagonal symmetry of the zinc lattice. The purple spot representing region 6 will coincide with the fluorescent green spot representing region 3 after rotating about 100° counterclockwise around the polar axis of the <0001>. Similarly, the dark blue spot will coincide with the fluorescent green spot with a 120° rotation clockwise around the polar axis of the <0001>.

Based on the polar figures of {11-20} and {10-10}, the three orange-colored spots representing region 1 (orthorhombic dendritic arm spangle) are approximately equidistantly distributed and close to the symmetrical center of the circular center, which indicates that the <0001> orientation of the grains is almost parallel to the surface of the steel matrix, resulting in the three independent spots representing the <11-20> and <10-10> orientations projecting in the lower hemisphere. The spots representing regions 5, 7, and 8 show similar characteristics, which proves that they belong to the same spangles type. Similarly, in the pole figure of (10-10) crystal planes, the yellow, blue, light blue, and light purple spots representing the regions 1, 5, 7, 8 (orthogonal dendrite arm spangles) can achieve a less strict crystallographic coincidence with a simple rotation around the polar axis <0001>. However, the coincidence is not equal to the consistency in crystalline form, considering that the same lattice can achieve the consistency after at most three rotations around at most two coordinate axes according to the definition of Euler angle [29, 30]. Therefore, only one rotation can't lead to consistency in the crystalline form. There could be a slight angle difference. Based on the above analysis, the formation of different morphologies of spangles is caused by the different crystallographic orientation of the crystal grains compared to that of the steel base surface.

According to the change of the orientation angle, the spangle's morphology gradually evolves.

In order to interpret the orientations of spangles in an intuitive way, the crystal orientations of every grain were configured and redrawn based on their Euler angles, as shown in Figure 8 (a). The basal planes (0001) of grain 3, 4, and 6 are almost parallel to the steel base plane, while the prismatic plane of grain 8 is almost parallel to the steel base plane. According to the 3D orientation reconstruction figure, the base plane of the feathery spangle is approximately parallel to the steel base plane, the former of the orthogonal dendrite arm spangle is approximately perpendicular to the latter, and the base plane of the ridged spangle is in the middle. The result in this figure is consistent with the analysis of the orientation pole figure of the three types of spangles.

The rotation axis and the corresponding rotation angles were calculated based on Euler angles to quantitatively investigate the orientation relationship among the grains, and the results are listed in Table 2. The rotation angle among grain 5 and grain 6 is 92.3°, with the corresponding axis being (-3-10). It means that grain 5 will coincide with grain 6 by rotating around the rotation axis (-3-10) by 92.3°. For other grains, such as grains 1-2, 1-4, 2-3, and 1-5 respectively has 69°, 87.3°, 59.5°, and 20.1° rotation angle. The misorientation of different types of spangles is large, while that of the same type is relatively small. Feathery spangles are in regions 3, 4, and 6, where the rotation angle among 3-4 and 4-6 is only 10.5° and 14.9° around the different rotation axis. The rotation angle among region 2 (ridged spangles) and region 6 (feathery spangles) is 54.2°, smaller than the rotation angle of 81.1° among region 1(orthogonal dendrite arm spangles) and region 6. It demonstrates that the ridged spangle is a transition state among the feathery spangle and the orthogonal dendrite arm spangle. The orientation analysis among spangles revealed that spangles morphology is decided by the relative positions of the dense rows of hexagonal crystal structures of the spangles compared
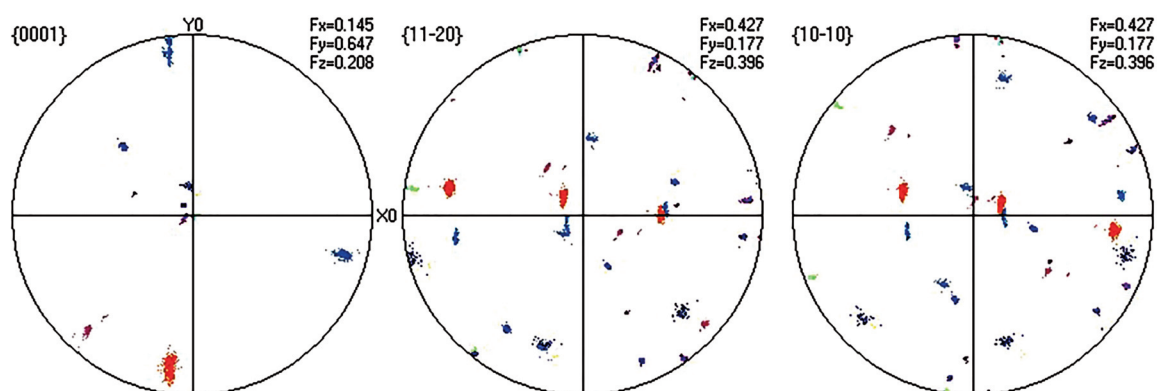

Figure 9. <0001>, <11-20>, and <10-10> orientation pole figures of grains in the EBSD region

with the steel base plane. The rule can be illustrated by the relative angular relationship among the <0001> spangle orientation and steel base plane: As the angle among <0001> orientation of the grain and the steel base plane decreases, the spangles morphology changes from feathery to ridged, and ends up with the orthogonal dendrite arm.

According to crystallographic studies in the same grain, even though the crystal orientations can be the same, there will still be misorientation [31]. Some straight lines were drawn (marked by numbers ①-⑨) in different spangles in order to characterize the grain orientation in an intuitive manner. As shown in Figure 10, the study focuses on the dendrite orientation distribution along the arrow

Table 2. *Calculated angle and the corresponding axis of rotation among the spangles*

Grain		Rotation angle (°)	Rotation axis
1	2	69.0	(-3-10)
	3	80.9	(-230)
	4	87.3	(320)
	5	20.1	(230)
	6	81.1	(70-1)
	7	84.1	(3-10)
	8	37.4	(12,2,3)
2	3	59.5	(-3-10)
	4	49.4	(3-6-1)
	5	49.0	(93-1)
	6	54.2	(-1-10)
	7	50.0	(-410)
	8	90.5	(-8-4-1)
3	4	10.5	(210)
	5	91.2	(410)
	6	16.0	(232)
	7	80.4	(-3-20)
	8	87.1	(13,-3,2)
4	5	83.7	(110)
	6	14.9	(-324)
	7	90.3	(-4-10)
	8	85.4	(-3-20)
5	6	92.3	(-3-10)
	7	68.6	(-320)
	8	55.3	(-50-1)
6	7	87.1	(-3-20)
	8	78.7	(210)
7	8	64.1	(0-10)

of the straight lines. As shown in Table 3, together with BSE Figure 8 (b), the misorientation of different dendrites varies a lot. In region 1 with orthogonal dendrite arm spangles, the secondary dendrite arm ④ is perpendicular to the primary dendrite arm ① while the average rate of misorientation of ④ is higher than that of ①. Similarly, ③ is perpendicular to the main dendrite arm ②, while the average rate of misorientation of ③ is higher than that of ②. In region 2 with ridged spangles, the straight lines ⑤ and ⑥ represent the direction of the primary and the secondary dendrite arm, respectively. Their average rates of misorientation are similar. However, the average rate of misorientation of ⑦, which is perpendicular to the primary dendrite arm, becomes smaller and more stable compared to that of ⑤ and ⑥. Both the maximum orientation change rate and the maximum misorientation were relatively low. In region 6 with feathery spangles, the straight line ⑨ is perpendicular to the secondary dendrite arm ⑧, and its average rate of misorientation is twice that of ⑧ . Along the dendrite arm, the orientation of the dendrite changes tends to be slow and smooth, while the orientation across the dendrite arm changes grammatically and irregularly. In terms of the causes, during the solidification process, the primary dendrite arms formed first, which will interfere with the formation and growth of secondary dendrites. As the dendrite grows, adjacent unit cells will solidify, resulting in small misorientation. The misorientation among two adjacent points across the dendrites may have accumulated several dendrite deviations and thus become large.
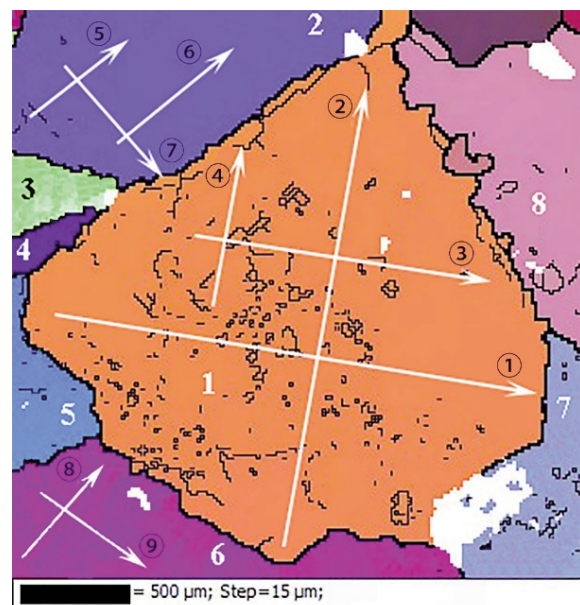

Figure 10. *Map of misorientation within spangles*

Table 3. Dendrite misorientation along straight lines

Line number	Distance(μm)	Average orientation change rate*1000 (°/μm)	Maximum orientation change rate (°/μm)	Head-to-tail misorientation (°)	Maximum misorientation (°)
①	2478.823	0.4655	0.1741	1.1539	5.9438
②	2442.609	1.6072	0.0465	3.9257	3.9257
③	1020.624	2.7365	0.0860	2.7929	3.3682
④	705.625	0.5444	0.0222	0.3841	1.5640
⑤	713.970	1.4042	0.3333	1.0026	1.5627
⑥	937.462	1.5323	0.0395	1.4364	1.8788
⑦	615.183	1.2936	0.0229	0.7958	1.1678
⑧	234.853	0.9737	0.0064	0.2287	0.3930
⑨	442.279	1.7421	0.0706	0.7705	2.3297

3.3 Effect of Sn on crystal orientation

Through the composition analysis and EBSD analysis of the zinc coating, the spangles morphology gradually changed from feathery to orthogonal dendrite arm with the increase of the Sn content on the surface. Besides, the crystal orientation also influences the spangle's morphology. When the angle among the <0001> orientation of the spangle crystal and the normal of the steel base surface changes from 0° to 90°, feathery spangles change to orthogonal dendrite arms spangles. Considering that pure zinc coatings don't have preferential orientation, there must be a time sequence of the influence of Sn and the crystal orientation on spangles morphology. The addition of Sn affects the orientation of the spangle. However, in the process of solidification [5], the composition of the dendrite is almost pure zinc. During the process, Sn-rich residual liquid solidifies at last. Therefore, a key problem of nucleation kinetics is how Sn affects the orientation of dendrites in the liquid phase, which cannot be clarified for the time being.

4. Conclusions

1. In the Zn-Sn zinc bath, a little Sn will cause significant element surface segregation. With the increase of Sn on the surface, feathery spangles gradually become orthogonal dendrite arm spangles.

2. The dendrite of spangles repulses Sn during the growth and solidification process, resulting in the continuous Sn enrichment in the remaining molten. In the end, it will solidify in the form of a metastable divorced eutectic structure among the dendrite arms. The Sn content in the acicular Sn-rich phase is significantly lower than that of the bulk and strip tin-rich phases, whose compositions are very similar. The morphology of the tin-rich phase is related to the wettability and relative position of the residual liquid and the primary Zn during the solidification process.

3. The addition of Sn dramatically changed the crystal orientation of η-Zn. The coating surface preferred orientation changes from <0001> to <10-10>.

4. There is a relatively small misorientation within a spangle grain. The orientation changes along the dendrite arm are relatively smooth and low, while the orientation changes perpendicular to the dendrite arm has a saltatory and irregular fluctuation. The internal orientation may be related to the macroscopic direction of the dendrite arms. The misorientation among grains of different spangles types tends to be large while that within the same type is smaller. As the feathery spangles change to orthogonal dendrite arms spangles, the rotation angle required for their coincidence also grows.

5. The addition of Sn affects the crystal orientation of spangles so that the morphology of the coating surface has changed. The feathery spangle has a preferred orientation <0001>, while the orthogonal dendrite spangle has a preferred orientation <11-20>. For the rest spangles, the orientation varies among them. When the angle among the <0001> orientation of the spangle crystal and the normal of the steel base surface changes from 0° to 90°, feathery spangles change to orthogonal dendrite arms spangles.

Acknowledgements

References

[1] G. Vourlias, N. Pistofidis, G. Stergioudis, Phys. Status Solidi. A, 201 (7) (2004) 1518-1527.

[2] G. Vourlias, N. Pistofidis, G. Stergioudis, Cryst. Res. Technol., 39 (1) (2004) 23-29.

[3] F.A. Fasoyinu, F. Weinberg, Metall. Trans. B, 21 (3) (1990) 549-558.

[4] M. Godzsák, G. Lévai, K. Vad, J. Min. Metall. Sect. B-Metall., 53 (2017) 28-28.

[5] J. Strutzenberger, J. Faderl, Metall. Mater. Trans. A, 29 (2) (1998) 631-646.

[6] A. Sémoroz, L. Strezov, M. Rappaz, Metall. Mater. Trans. A, 33 (8) (2002) 2685-2694.

[7] A. Sémoroz, L. Strezov, M. Rappaz, Metall. Mater. Trans. A, 33 (8) (2002) 2695-2701.

[8] M. Zapponi, A. Quiroga, T. Pérez, Surf. Coat. Technol., 122 (1) (1999) 18-20.

[9] A. Sémoroz, Y. Durandet, M. Rappaz, Acta Mater., 49 (3) (2001) 529-541.

[10] J.T. Lu, X.H. Wang, C.S. Che, T. Nonferr. Metal. Soc., 17 (2) (2007) 351-356.

[11] J.T. Lu, X.H. Wang, C.S. Che, Surf. Interface Anal., 39 (10) (2007) 805-808.

[12] R.Y. Chen, D. Yuen, Metall. Mater. Trans. A, 43 (12) (2012) 4711-4723.

[13] H. Asgari, M.R. Toroghinejad, M.A. Golozar, J. Mater. Process. Technol., 198 (1-3) (2008) 54-59.

[14] S. Peng, J.T. Lu, C.S. Che, Appl. Surf. Sci., 256 (16) (2010) 5015-5020.

[15] S. Peng, S.K. Xie, J.T. Lu, J. Alloys Compd., 728 (2017) 1002-1008.

[16] S. Peng, S.K. Xie, F. Xiao, Corros. Sci., (2019) 108237.

[17] A. Quiroga, S. Claessens, B. Gay, Metal. Mater. Trans. A, 35 (11) (2004) 3543-3550.

[18] P.R. Seré, J.D. Culcasi, C.I. Elsner, Surf. Coat. Technol., 122 (2-3) (1999) 143-149.

[19] Z. Moser, J. Dutkiewicz, W. Gasior, J. Phase Equilib.Diff., 6 (4) (1985) 330-334.

[20] C.M.L. Wu, C.M.T. Law, D.Q. Yu, J. Electron. Mater., 32 (2) (2003) 63-69.

[21] L.R. Garcia, R. Wislei Osório, L.C. Peixoto, J. Electron. Mater., 38 (11) (2009) 2405-2414.

[22] T. Wataya, M. Yoshikawa, T. Tanaka, J. Jpn. I. Met., 67 (11) (2003) 643-646.

[23] M. Sun, Y. Yang, M. Luo, Acta Metall. Sin. (Engl. Lett.), 28 (2015) 1183-1189.

[24] P. Cheng, N. Dai, N. Zhong, Corros. Eng. Sci. Technol., 55 (2020) 232-240.

[25] R.E. Fraley, MS Thesis, Lehigh University, USA, 1994.

[26] P.K.K. Nayar, Scripta Metall., 13 (12) (1979) 1115-1116.

[27] R. Lück, E. Hering, Scripta Metall., 2 (11) (1968) 625-628.

[28] L.F. Zagonel, N. Barrett, O. Renault, Surf. Interface Anal., 40 (13) (2008) 1709-1712.

[29] N.J. Park, S.J. Jin, C.W. Jea, Solid State Phenom., 105 (2005) 213-218.

[30] T.M. Ivanova, V.N. Serebryanyi, Inorg. Mater., 54 (15) 2019 1477-1482.

[31] T.H. Behm, C. Funke, H.J. Möller, Surf. Interface Anal., 45 (4) (2013) 781-786

UTICAJ MORFOLOGIJE I KRISTALNE ORIJENTACIJE DENDRITA KOD Zn-0.5Sn PREVLAKE DOBIJENE VRUĆOM GALVANIZACIJOM

L. Zhai [a], H.-P. Peng [a,b,c,*], Y. Liu [b,c], Y. Lei [a], S. Deng [a], X.-P. Su [b,c]

[a] Đangsu Glavna laboratorija za nauku i tehnologiju površine materijala,
Čangzou univerzitet, Đangsu, NR Kina
[b] Đangsu glavna laboratorija za skladištenje i transport nafte i gasa, Čangzou univerzitet, Đangsu, NR Kina
[c] Đangsu kolaborativni inovacioni centar za fotonaponsku nauku i inženjerstvo,
Čangzou univerzitet, Đangsu, NR Kina

Apstrakt

Ispitivanje morfologije površine i orijentacije kristala u Zn-0.5Sn prevlaci moglo bi dati smernice za poboljšanje površinskih karakteristika prevlaka dobijenih vrućom galvanizacijom. U ovom radu korišćeni su skenirajući elektronski mikroskop (SEM) i energetski disperzivni spektometar (EDS) za analizu uticaj morfologije i kristalne orijentacije dendrita (spangles – kristali oblika pahuljice/zvezde). Tekstura površine prevlake analizirana je rentgenskom difrakcijom (XRD). Elektronska difrakcija povratnim elktronskim raspršenjem korišćena je da bi se analizirala orijentacija kristala oblika pahuljice/zvezde. Rezultati pokazuju da dolazi do segregacije kalaja među kristalima oblika pahuljice/zvezde koji su dendritne strukture dok metastabilne razdvojene eutektičke strukture mogu da se održe u fazi bogatoj kalajem, gde je sastav veoma sličan. Orijentacija kristala oblika pahuljice/zvezde utiče na njihovu morfologiju i dovodi do formiranja dendritne grane kristala koja je u obliku pera, grebena i ortogonalna. Kada se ugao između <0001> orijentacije kristala i normale površine čelične osnove promeni od 0° to 90°, kristali u obliku pera se menjaju u ortogonalne dendritne grane. Misorijentacija unutar kristala je mala, ali je među kristalima velika. Promene orijentacije u pravcu dendritne grane su relativno glatke i slabe, dok promene orijentacije koje su vertikalne u odnosu na dendritnu granu imaju nepravilnu i skokovitu fluktuaciju.

Ključne reči: Vruća galvanizacija; Kristal oblika pahuljice/zvezde; Orijentacija kristala; Elektronska difrakcija povratnim elktronskim raspršenjem